Kinetic roughening of charge spreading in a two-dimensional silicon nanocrystal network detected by electrostatic force microscopy

R. Dianoux,[1,2,*] H. J. H. Smilde,[3] F. Marchi,[4,5,†] N. Buffet,[3] P. Mur,[3] F. Comin,[1] and J. Chevrier[1,4,5]
[1]*ESRF, B.P. 220, 38043 Grenoble cedex 9, France*
[2]*CEA, DRFMC/SP2M/SiNaPS, 17 avenue des Martyrs, 38054 Grenoble cedex 9, France*
[3]*CEA-DRT, LETI/DTS, 17 avenue des Martyrs, 38054 Grenoble cedex 9, France*
[4]*CNRS/LEPES, 25 avenue des Martyrs, 38042 Grenoble cedex 9, France*
[5]*Université Joseph Fourier, B.P. 53, 38041 Grenoble cedex 9, France*
(Received 14 May 2004; revised manuscript received 15 October 2004; published 8 March 2005)

The charging dynamics of silicon nanocrystals embedded in a silicon-dioxide matrix is studied using electrostatic force microscopy. Varying the average oxygen content of the silicon-rich–oxide samples, different charge-spreading behaviors are observed. Three kinds of behavior are distinguished: charge confinement in isolated clusters (insulating), spreading via a network of clusters and metallic. They relate to the local material composition with a threshold silicon/silicon oxide ratio for conduction, a characteristic of percolation. Close to this threshold, *in situ* and real-time experimental charge spreading on the timescale of several hours in a two-dimensional silicon nanocrystal network is evidenced, with an irreversible evolution of a rough borderline of the electron cloud.

DOI: 10.1103/PhysRevB.71.125303 PACS number(s): 73.63.Bd, 68.43.Jk, 73.23.Hk, 07.79.Lh

I. INTRODUCTION

The efficient and reproducible elaboration of dense and homogeneous layers of silicon nanocrystals in combination with local and sensitive (routinely down to a few electrons) electrostatic force measurement techniques has opened the way to investigations of the collective behavior of charges in these 2D disordered layers at the nanoscale. In these systems, the electrostatic interaction energy is much larger than the thermal and zero-point motion energies due to confinement.

Silicon nanocrystals (Si-nc) embedded in a silicon dioxide matrix have attracted attention in the past decade for their applications in nanoelectronics. They present interesting properties in the field of optical devices such as a high-efficiency light source[1] for telecommunications ($\lambda = 1.54\ \mu$m) and in efficient and chemically more stable solar cells.[2] Also, they present promising data storage capabilities used as a floating gate in nonvolatile memories.[3,4] In the latter case, advantage has been taken of the reduced mobility to reach remarkably long charge retention times, coupled to enhanced read-write capabilities.[5] For these applications, an accurate control of the local material composition is necessary, because the size and density of the Si-nc, the intercrystal spacing, and oxide quality determine the mobility or confinement of the charges injected in the Si-nc network. Standard techniques including Fourier transform infrared (FTIR) spectroscopy and ellipsometry are routinely applied to check for the material properties of the prepared samples. However, these techniques probe the properties rather macroscopically, compared to the nanometer-sized Si-nc.

This article addresses the question of charge transport at the nanoscale in these Si-nc networks. We provide experimental evidence for all characteristic regimes. Two extreme regimes of charge transport are identified: as the initial silicon concentration is very close to that of stoichiometric SiO_2, one expects very few Si-nc. Therefore a collective behavior of injected charges very close to that of a SiO_2 layer is observed: an insulating behavior with a static two-dimensional (2D) disk shape of charges. Oppositely, at high silicon content, one expects a metallic regime in the 2D interconnected Si layer. The intermediate regime is reminiscent of the problem of 2D percolation, however with a very important difference: we are concerned here with the spreading of charges inside a 2D disordered layer at the nanometer scale. Therefore, the electron interaction, or Hartree term, due to the space charge is a key factor in the spatial distribution of the charges. This space charge has in fact no screening charge to cancel its electric field, making it the driving force for charge spreading. A specific point of this work is hence the intrinsic contributions of disorder at the nanoscale and of a long-range, unscreened electrostatic interaction on the electron distribution. The irregular spreading of the electron cloud relates to kinetic roughening,[6] a phenomenon commonly observed in systems such as the slow combustion of paper[7] or epitaxial growth,[8] but until now never with charges.

The atomic force microscope[9] and the related electrostatic force microscope (EFM) are accurate tools for the local and nondestructive investigation of Si-nc. They have proven their performance for local charge injection and detection.[10–14] A resolution down to some tens of electrons in ambient conditions[15] and a spatial resolution amounting to less than 100 nm is reached. Charging of assemblies of quantum dots has been studied on other systems,[16,17] as well as charging of single quantum dots.[18,19] Ultimately, the AFM has proven single-charge detection.[20]

In this article, we investigate the different charge spreading behaviors related to the local material composition of the Si-nc layers using the EFM technique. First, the preparation of the samples and spectroscopic ellipsometry analyses are described, after which the EFM technique and the experi-

 ©2005 The American Physical Society

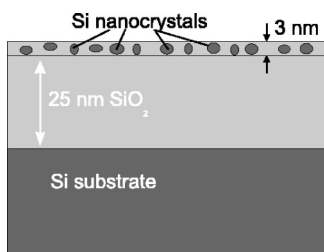

FIG. 1. Sample geometry.

mental conditions are clarified. The three behaviors of charge spreading are experimentally evidenced. We demonstrate a spreading of the charges via the network of Si-nc, with a kinetic roughening of the electron cloud on the time scale of several hours.

II. EXPERIMENT

To avoid leakage of charge injected in the nanocrystals to the grounded substrate, an insulating 25-nm-thick, high-quality SiO_2 layer is first thermally grown on (100)-oriented silicon substrates (impurity concentration 10^{-15} at. cm^{-3}). One sample undergoes no further preparation and serves as a reference for comparison with samples containing Si-nc. A 3-nm-thick silicon-rich-oxide[21,22] (SRO) layer is grown on top of the 25 nm SiO_2 by low-pressure chemical vapor deposition (LPCVD). Using a substrate temperature of 515 °C and a total gas pressure of 1000 mTorr, the two precursor gases SiH_4 and N_2O react, and an understoichiometric amorphous SiO_x film ($x<2$) is deposited. The deposition is followed by a 10-min rapid thermal annealing at 1000 °C under nitrogen at ambient pressure. This induces a phase separation of the amorphous SRO film, resulting in the precipitation of crystalline silicon nanocrystals in a silica matrix (see Fig. 1 for the sample geometry). The progress of the phase separation is examined using FTIR analysis on the -O-Si-O- stretching mode. Its vibration frequency is found at 1080 cm^{-1} for stoichiometric SiO_2 and shifts to smaller values for understoichiometric SiO_x (incomplete phase separation).

The density and size of the Si-nc embedded in a SiO_2 matrix thus wise obtained depend critically on the ratio of the gas fluxes, $\gamma=[N_2O]/[SiH_4]$, used during LPCVD. Previous high-resolution transmission electron microscopy studies have shown that Si-nc with a typical lateral dimension of 4–6 nm are formed, with an estimated density between 10^{11} and 10^{12} cm^{-2} Si-nc (Ref. 23).

Spectroscopic ellipsometry analysis is performed to determine the fraction of Si-nc in the SiO_2 matrix. The data are fitted with Bruggeman's effective-medium approach using the densities of crystalline silicon and of SiO_2 and their dielectric constants. This provides an estimate of the respective volume fractions. In addition to the reference sample, three different gas ratios are used for the fabrication of the samples: $\gamma=0.3$ (sample S1), 0.5 (sample S2), and 0.9 (sample S3). The corresponding volumic fractions $[Si/SiO_2]$, x parameters and fitted layer thickness from characterization with ellipsometry are summarized in Table I.

TABLE I. Ellipsometry analyses of the three Si-nc samples.

Sample	S1	S2	S3
$[Si]/[SiO_2]$ relative volumes	40/60	8/92	6/94
Atomic concentration x (=O/Si)	0.81	1.67	1.77
Thickness (nm)	2.4	2.8	4.4

Experiments are carried out in ambient temperature and pressure conditions using a commercial AFM.[24] Throughout the experiments, a permanent flux of nitrogen ensures a low relative humidity (RH: 15%) and avoids sample contamination, electrochemical reactions during charging, and charge evacuation paths on the surface. Rectangular, W_2C-coated tips[25] are used for sample charging and EFM characterization. The tips have spring constants ranging from 0.3 to 0.7 N/m and resonance frequencies between 28 and 41 kHz (manufacturer's data). The soft cantilevers ensure an enhanced detection. Indeed, the smallest detectable force gradient is[26] $\partial F_{min}/\partial z=(1/a_0Q)\sqrt{27k_BTBk/\omega_0Q}$, where Q is the quality factor, a_0 is the free oscillating amplitude, k_B is the Boltzman constant, T is the temperature, k is the cantilever stiffness, B is the bandwidth, and ω_0 is the angular resonance frequency. The minimum detectable force gradient is therefore proportional to the square root of the spring constant.

Charge is successively injected and detected with the same AFM tip. The AFM is operated in dynamic mode, near the resonance frequency of the cantilever. For the injection, the scan is stopped in the middle of the image and the tip is brought into contact with the sample surface by reducing the amplitude setpoint near to zero. A voltage in the range of ±0–10 V is applied to the tip while the substrate is kept grounded. The injection time is varied between 1 ms and 10 s. Immediately after charging, EFM scanning is resumed in a double-pass method. A first scan line records the surface topography. Then, the tip is retracted a few tens of nanometers (in our case 50 nm) with respect to the topography, the feedback loop is deactivated, and a second scan line records the phase of oscillation compared to the mechanical excitation at a constant tip-sample distance.[27] This phase is referred to as the EFM signal. Excess charges at the surface create an additional electrostatic force gradient, which is detected by the tip. This positive gradient (attractive force) increases the phase lag, resulting in a darker area in the EFM image.

As established in a previous publication,[15] one can provide a rough but robust and highly reproducible estimate of the number of electrons in a single cluster after injection. Based on the measured phase lag and using a parallel-plane geometrical approximation, one finds a 2D electron density in the charged area that is less or close to the Si-nc density. Directly from these experimental conclusions, the 2D electron cloud imaged by EFM will then be described as an area of uniformly charged network of nanocrystals with a single electron per crystal at maximum. This clearly emphasizes a strong parallel with the usual descrip-

tion of the single-electron transistor (SET, orthodox model[28]) including charging effects due to the Coulomb blockade, a key parameter controlling the charge states of the Si-nc network.

III. RESULTS

EFM images of the three samples prepared with increasing γ ratio are shown in Fig. 2.

Sample S1, which contains a high fraction of silicon in the top layer (40% in volume, see Table I), exhibits a metallic behavior, as seen in Fig. 2(a): as soon as deposited on the surface (conditions: -10 V/1 s), charges disappear on a time scale shorter than that of the scanning of the image (a few minutes). We assume that for a high density of Si-nc the silicon offers a percolation path, allowing the charges to spread immediately out from the injection site over the surface. Hence, the AFM is not the appropriate tool to measure charge spreading on such a sample. Figure 2(b) depicts the behavior of sample S2, which presents a low density of Si-nc (volumic fraction of silicon in the top layer: 8%). Charges are well localized around the injection site and may be detected more than 2 h after injection, with injection conditions of -10 V/10 s. The specificity of this sample lies in the rough edges of the charged area as well as a slow, sideward evolution of these edges.

The behavior of sample S3 is shown in Fig. 2(c): the charged area has a circular shape, with a typical diameter of less than a micron. Here, the charging conditions are -8 V/0.5 s. Once injected, the charges remain strongly localized in the nanocrystals. Even after more than an hour, no spreading is observed; i.e., there is no increase of the radius and no development of irregularity in the disk shape. It is clear in the investigated samples that the absence of charge spreading and the well-defined disk shape of the charge cloud are always simultaneously observed. With a volumic fraction of Si of 6% in the SRO layer, a lower density of Si-nc is prepared. It is assumed that the Si-nc are separated by one to a few nanometers of SiO_2. This kind of sample exhibits remarkable charge retention capabilities and therefore is of interest for application in nonvolatile floating-gate memories. Further investigations of this sample aiming at understanding the charge spreading mechanisms during injection will be the subject of a future publication.

The volumic fractions of silicon in the top layer are very close for samples S2 and S3 (respectively, 8% and 6%). The parameters of a strongly confining sample and a partially confining sample are therefore experimentally very close. This is further corroborated by a Si-nc sample not shown here with a volumic silicon fraction of 23%, which clearly exhibits a metallic behavior. We have encountered important difficulties in the preparation of samples exhibiting measurable charge spreading. The vast majority of samples are clearly either on the metallic side or on the strongly confining side. This is consistent with the existence of an extremely narrow window for samples presenting electron dynamics with a characteristic timescale of minutes to hours, in between conducting and strongly confining samples. An appar-

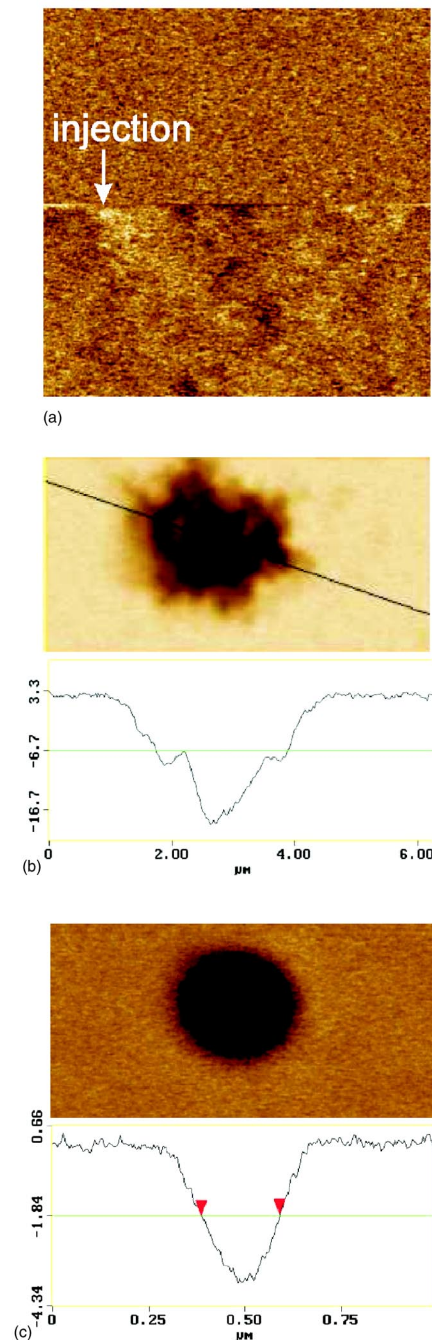

FIG. 2. (Color online) EFM signal (phase) of three Si-nc samples, excess charges appear dark: (a) Sample S1 displays a metallic behavior; charges are injected halfway through the scan and spread on a timescale inferior to the scan time. Injection is at -10 V/1 s; scan size is 4×4 μm^2. (b) Sample S2 displays a rough-edged behavior; charges distribute in clusters and flow between neighboring nanocrystals even after injection is completed. Injection is at -10 V/10 s; scan size is 3×6 μm^2. Below is a cross section of the charged area. (c) Sample S3 displays a circular-edged behavior; charges distribute homogeneously. They are trapped by the naocrystals and do not spread with time. Injection is at -8 V/0.5 s; scan size is 1×0.5 μm^2. Below is a cross section across the diameter of the charge spot.

ent abrupt transition from confining to metallic behavior as the oxygen content is varied is therefore characteristic of our observations. We are then led to the conclusion that, close to this transition, the Si-nc density and 2D spatial distribution very critically control the observed charge-spreading behavior. Using as a guideline the orthodox model established for a SET with a similar local geometry, we identify the mechanism at the root of these behaviors. It is essentially the intercrystal transition rate and the local influence of the Coulomb blockade on this intercrystal transition rate that determines the kinetics of electrons here. The properties of this transition rate are locally determined by the spatial distribution of clusters and by their detailed charge states.

Far from this conduction edge, the 2D map is either fully metallic or confining. If the transition rate is very high, electron kinetics is fast and the electron cloud spreads on a timescale shorter than the probe time. If the transition rate is very low, it leads to a nonmeasurable spreading on a timescale of hours, injection proceeds as the local electrostatic potential $V \gg e/C$. The electron cloud spreads only under the influence of the polarized tip, and it stops very rapidly away from the tip in a homogeneous way. Indeed the frontier of the electron cloud in the strongly confining regime is not rough at the scale of AFM measurement. In the confining case, the disorder in the Si-nc distribution at the nanometer scale has no influence on the shape of the 2D electron cloud. This extremely robust experimental result can be well understood using the limit of low density of Si-nc. In this limit, the intercrystal transition rate goes to zero, as the electron kinetics is essentially determined by the thick intercrystal silicon dioxide spacing, even if the initial electron trapping remains determined by the presence of Si-nc. The two regimes are separated by an abrupt transition that appears as a percolation threshold. It is close to this apparent percolation threshold that a third regime exists with a low intercluster transition rate, in which the interplay between the distribution of transition rates and single-electron charging effects results in charge spreading on a long timescale and with an increasingly rough borderline.

Before focusing on the electron cloud spreading in sample S2, we present a test experiment that compares the retention properties after injection of a plain oxide layer and of a comparable oxide layer with Si-nc. This is to directly check that Si-nc are clearly at the origin of the observed behaviors and it is not a property of the sole silicon layer. The same charging conditions of −10 V/10 s have been used to compare the retention characteristics of sample S2 and of the reference SiO_2 sample. The results are shown in Figs. 3 and 4, respectively. From Fig. 3(a) we remark that the injected charge is detectable more than 2 h after injection, whereas the retention time amounts to about 5 min in the case of the reference sample [see Fig. 4(a)]. This along with the long retention time of sample S3 confirms that the presence of the nanocrystals is essential to trap the charges and exhibit a long retention time.

In the following, we concentrate our investigations on sample S2 and demonstrate that charges spread irregularly through the neighboring Si-nc long after injection has ended, a phenomenon never observed up to this day. This sample offers the possibility to analyze how the Si-nc distribution at the nanometer scale can determine the shape of the injected electron cloud at the micrometer scale. These observations are studies of charge spreading mechanisms in assemblies of nanocrystals that are related to earlier theoretical works on transport in assemblies of dots with disorder.[29]

To investigate charge spreading in sample S2, we have superimposed the cross sections of the phase images taken over time on the same position (drift has been corrected). The position is shown by the line drawn across all images in Fig. 3(a) and the cross sections are plotted in 3(b), upper graph. The encircled area highlights a region where charges accumulate with time, as confirmed by the phase images, while other regions tend to depopulate with time. The lower, normalized phase graph shows that the general shape of the curve is not conserved and confirms the charge spreading to the encircled area, in which the signal augments with time. In comparison, the reference SiO_2 sample does not display any charge spreading. The cross sections plotted across the diameter of the phase images [Fig. 4(b)] decrease with time without spreading, as emphasized in the normalized graph. It is not clear whether charges spread laterally on the surface below te detection threshold (due, for example, to a very thin water rest layer) or diffuse to the substrate through the SiO_2 layer. The latter is corroborated by previous studies on thin Al_2O_3 films.[30]

Sample S2 displays some regions that are very stable and do not seem to evolve with time, while some micrometric areas are progressively filled with electrons to the detriment of others. This macroscopic roughness reflects the nanometric, highly inhomogeneous distribution of the Si-nc, which seem to agglomerate in clusters. The minimum spatial wavelength identified at the frontier of the electron cloud is about 50 nm. It is mainly determined by the EFM spatial resolution, which corresponds to the EFM lift height.

We remark that the regular evolution and long timescale of charge displacement in this regime is indicative for an electronic mechanism rather than a chemical modification. Moreover, reproducibility of the injection experiments over a period of 6 months demonstrates the chemical stability of the samples.

IV. DISCUSSION

The spreading behavior of sample S2 reflects a kinetic roughening of the electron cloud front in a disordered array (quenched disorder) of Si-nc, driven by the long-range, electron-electron repulsive force. To our knowledge, this is the first time that such a behavior is directly observed for an electron system, although its has been theoretically anticipated by Middleton and Wingreen[29] in this context. We will now describe the key mechanisms that root this behavior.

After completion of the injection, the 2D electron cloud is far from its equilibrium state, due to electrostatic repulsion in this dense cloud. Indeed, an estimate of the unscreened local electric field at intercrystal distance yields $e/(4\pi\epsilon_0\epsilon_{SiO_2}d^2)$

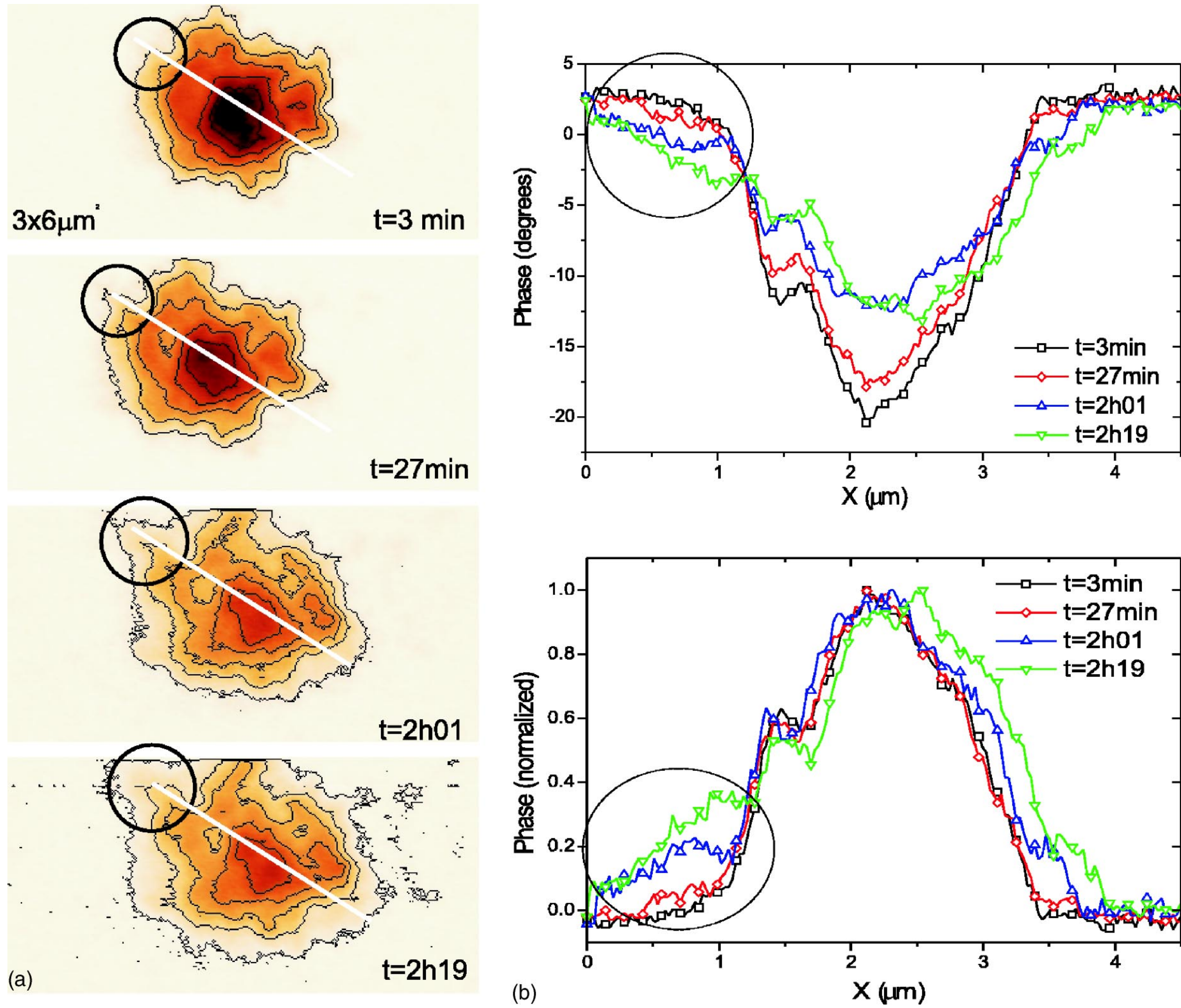

FIG. 3. (Color online) Evidence of charge spreading on sample S2. (a) Time evolution of the phase images over 2 h. Injection parameters are −10 V/10 s; image sizes are $3\times 6\ \mu m^2$. (b) Cross sections of the images as shown in. (a). The top graph presents the raw data and the bottom graph the normalized phase displaying the lateral spreading of the charges.

$=10^6-10^7$ V/m for a Si-nc density of $\approx 10^{12}\ cm^{-2}$. These are extremely high electrical fields, yet not high enough to deteriorate the silicon dioxide which electric breakdown occurs at over 10^9 V/m. The electrical force experienced by electrons especially at the borderline tends to the explosion of the electron cloud. The distribution of nanocrystals enables us to control the electron kinetics—i.e., not only to prevent this explosion, but also to slow it down to accessible timescales. We observe that it can introduce macroscopic intercrystal transition rate. Indeed, Coulomb blockade effects for sample S2 dominate intercrystal transition rates. In a simple approximation, the intercrystal capacitance is taken as a parallel plate capacitor $C=\epsilon_0\epsilon_{SiO_2}A/d$, with a Si-nc area of $A=\pi r^2$ ($2r=5$ nm is the diameter of the Si-nc) and an intercrystal distance of $d=1$ nm. This yields a capacitance $C=0.7$ aF and corresponds to a characteristic voltage e/C of 0.2 V. The intercrystal resistance R_t, calculated with the above geometry and using $\rho_{SiO_2}=10^{14-16}\ \Omega.cm$,[31] amounts to $5\times 10^{19}\ \Omega$. From the progress of several hundreds of nanometers of the electron front per hour, we estimate the characteristic transition time of an electron from one nanocrystal to the next to amount to $\tau=10$ s. These values relate very well in the frame of the orthodox SET theory,[28] in which the transition rate for one electron $(n=1)$ is expressed as

$$\tau^{-1}=\frac{1}{R_t e^2}\frac{-\Delta E^{+}}{1-\exp(\Delta E^{+}/k_B T)}.$$

In this, $\Delta E^{+}=-(1/2)[(e^2/2C)+eV_a]-(ne^2/2C)$ involves the energies associated with the transfer process, with relevant voltages of the order of 0.1 V. The calculated transfer time with our parameters amounts to the order of seconds. In a 1D approximation, this corresponds to a progression of the electron front of a few hundreds of nanometers per hour, all of which is in agreement with our experimental values. This is, however, in strong contrast with typical transition rates prepared in SETs that are around 1 GHz. Indeed, whereas the involved voltages are comparable, the tunneling resistance is 9 orders of magnitude larger than in the case of SETs, and accounts for the variation in the transition rate.

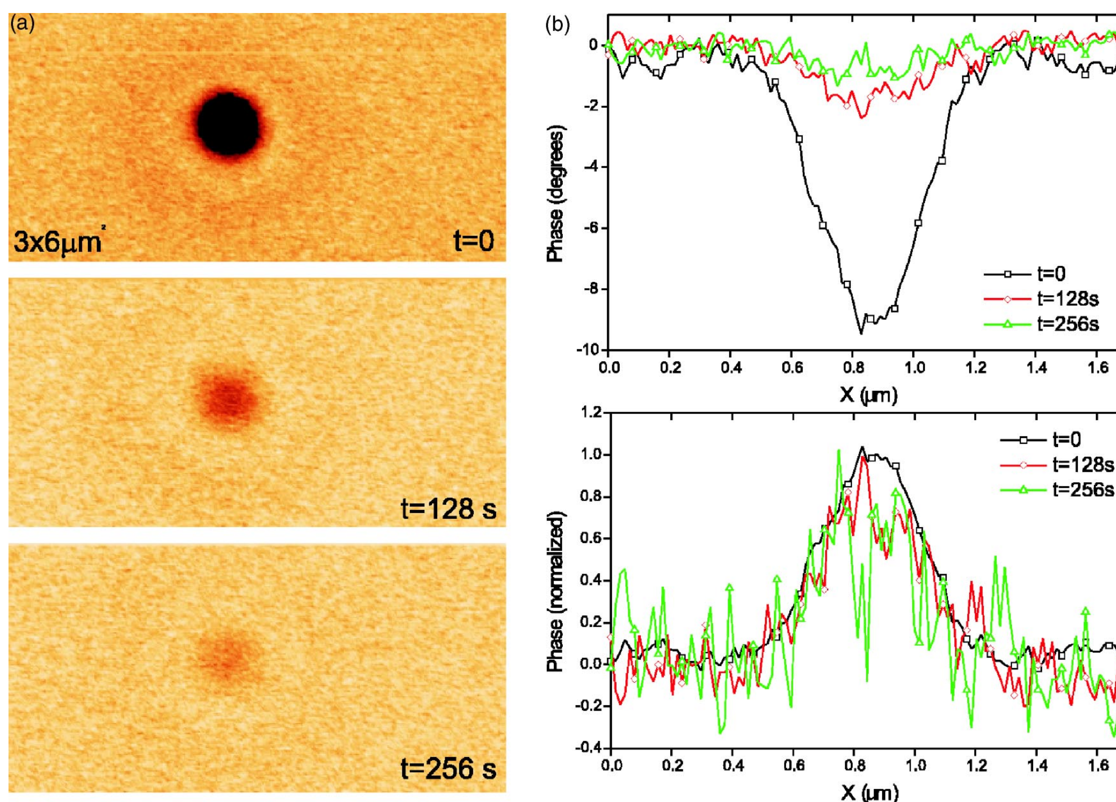

FIG. 4. (Color online) Evidence of charge localization on the reference SiO_2 sample. (a) Time evolution of the phase images over 256 s. Injection parameters are −10 V/10 s; image sizes are 2×4 μm^2. (b) Cross sections of the images as shown in (a). The top graph presents the raw data and the bottom graph the normalized phase exhibiting the conservation of the general shape of the phase.

This local transition rate depends very sensitively on the distribution of the Si-nc in the network, characterized by their sizes and the intercrystal distances. Moreover, this distribution introduces disorder in the problem at the nanoscale. As already mentioned, it is striking to observe that this disorder does not appear experimentally in the electron cloud shape in the strongly confining regime whereas the roughness of the electron front in the intermediate regime is a characteristic observation. In this last regime, electrons irreversibly redistribute to energetically lower-lying states with a characteristic kinetic time in the order of the second. The slow and continuous observed spreading shows that the disorder does not manifest itself only by a set of characteristic lengths that would describe, for instance, weak resistance Si-nc interconnections. In this case, although possibly rough, the electron cloud would invade the available Si-nc network at high speed, leading to an unobservable fast spreading for AFM. We have in fact observed the latter behavior in randomly interconnected silicon dots prepared by electron beam lithography. In the present experimental results, the disorder appears to result in a set of timescales for electron hopping, which is spatially and randomly distributed at the nanometer scale. Although not identical, this analysis of our experimental results is then very close to the theoretical arguments presented by Middleton and Wingreen.[29] They have studied in detail how the disorder due to offset charges combined with a local charging effect due to Coulomb blockade should lead to kinetic roughening of the electron front displaced in a 2D regular network of capacitances and resistances. Furthermore, kinetic roughening of the moving surface of a crystal during MBE growth has been observed experimentally in the past[32] and thoroughly analyzed.[33] The origin in this case lies in the relevance of noise at the nanometer scale due to random deposition of atoms at the atomic scale. In our experiments, the origin of kinetic roughening is in the combination of the random distribution of Si-nc and of a charging effect described by a ratio e/C that is significant compared to the average voltage drop when moving from one crystal to another, away from the cloud center. As the precise local configuration of charged clusters determines the transition rate between two crystals, the electron kinetics becomes very sensitive to the disorder in the spatial distribution of the nanocrystals, in their size, and in their intercrystal distance. This is the origin of the observed roughness that develops during spreading. Therefore, this phenomenon presents the essential characteristic of kinetic roughening. We believe that this is the first time that the proposed relevance of kinetic roughening for charge spreading in the presence of quenched disorder[29] is demonstrated experimentally, by *in situ* and real-time imaging.

V. CONCLUSION

We have studied samples containing silicon nanocrystals embedded in a silica matrix using electrostatic force microscopy. In such structures, the electric transport properties depend sensitively on the sample preparation conditions. Three kinds of charge spreading behavior are distinguished using

EFM and related to the nanocrystal density. Large concentrations of buried silicon in silicon dioxide lead to a characteristic metallic behavior. Low concentrations exhibit a clear confining behavior: injection of charges from the tip forms a two-dimensional cloud with an exact disk shape that does not spread with time. At a slightly higher silicon concentration, the injected electron cloud presents an irregular borderline, which spreads out onto the surface on a timescale of the hour. We explain this until now unobserved phenomenon with a redistribution of the electrons through clusters of nanocrystals to reach a more stable energetic state. This behavior qualifies as kinetic roughening because the repulsive electron interaction (Hartree term) leads to an irreversible charge spreading into a disordered array of silicon nanocrystals which would be termed as quenched noise within the framework of kinetic roughening. The transition from a metallic to an insulating behavior is critically dependent on the nanocrystal density.

ACKNOWLEDGMENTS

The authors acknowledge N. Rochat for the FTIR and ellipsometry analysis. This work has been carried out in the frame of the French national project ACI NanoSciences "Sub-PicoNewton" and in the frame of CEA-LETI/CPMA collaboration, with PLATO Organization teams and tools. Some of the data processing has been carried out with the freeware WSxM, distributed by Nanotec (Spain). http://www.nanotec.es

---

*Electronic address: dianoux@esrf.fr
†Electronic address: marchi@cnrs.grenoble.fr

[1] M. E. Castagna, S. Coffa, M. Monaco, L. Caristia, A. Messina, R. Mangano, and C. Bongiorno, Physica E (Amsterdam) **16**, 547 (2003).
[2] J. De La Torre *et al.*, Physica E (Amsterdam) **16**, 326 (2003).
[3] S. Tiwari, F. Rana, H. Hanafi, A. Hartstein, E. F. Crabbe, and K. Chan, Appl. Phys. Lett. **68**, 1377 (1996).
[4] A. Kohno, H. Murakami, M. Ikeda, S. Miyazaki, and M. Hirose, Jpn. J. Appl. Phys., Part 2 **40**, L721 (2001).
[5] S. Banerjee, S. Huang, T. Yamanaka, and S. Oda, J. Vac. Sci. Technol. B **20**, 1135 (2002).
[6] M. Kardar, G. Parisi, and Y. C. Zhang, Phys. Rev. Lett. **56**, 889 (1986).
[7] J. Maunuksela, M. Myllys, O. P. Kahkonen, J. Timonen, N. Provatas, M. J. Alava, and T. Ala-Nissila, Phys. Rev. Lett. **79**, 1515 (1997).
[8] S. Vézian, F. Natali, F. Semond, and J. Massies, Phys. Rev. B **69**, 125329 (2004).
[9] G. Binnig, C. F. Quate, and C. Gerber, Phys. Rev. Lett. **56**, 930 (1986).
[10] B. D. Terris, J. E. Stern, D. Rugar, and H. J. Mamin, Phys. Rev. Lett. **63**, 2669 (1989).
[11] C. Schönenberger, Phys. Rev. B **45**, 3861 (1992).
[12] R. C. Barrett and C. F. Quate, J. Appl. Phys. **70**, 2725 (1991).
[13] K. Domansky, Y. Leng, C. C. Williams, J. Janata, and D. Petelenz, Appl. Phys. Lett. **63**, 1513 (1993).
[14] Y. Sugawara, Y. Fukano, T. Uchihashi, T. Okusako, S. Morita, Y. Yamanishi, T. Oasa, and T. Okada, J. Vac. Sci. Technol. B **12**, 1627 (1994).
[15] C. Guillemot, P. Budeau, J. Chevrier, F. Marchi, F. Comin, C. Alandi, F. Bertin, N. Buffet, C. Wyon, and P. Mur, Europhys. Lett. **59**, 566 (2002).
[16] D. M. Schaadt, E. T. Yu, S. Sankar, and A. E. Berkowitz, Appl. Phys. Lett. **74**, 472 (1999).
[17] N. Shimizu, M. Ikeda, E. Yoshida, H. Murakami, S. Miyazaki, and M. Hirose, Jpn. J. Appl. Phys., Part 1 **39**, 2318 (2000).
[18] E. A. Boer, L. D. Bell, M. L. Brongersma, H. A. Atwater, M. L. Ostraat, and R. C. Flagan, Appl. Phys. Lett. **78**, 3133 (2001).
[19] T. Mélin, D. Deresmes, and D. Stiévenard, Appl. Phys. Lett. **81**, 5054 (2002).
[20] L. J. Klein and C. C. Williams, Appl. Phys. Lett. **81**, 4589 (2002).
[21] M. L. Hitchman and J. Kane, J. Cryst. Growth **55**, 485 (1981).
[22] W. Y. Ching, Phys. Rev. B **26**, 6610 (1982).
[23] N. Buffet, P. Mur, B. De Salvo, and M. N. Sémeria, *Proceedings of the IEEE Conference on Nanotechnology*, 26–28 August 2002, Washington, DC, USA, p. 269–272.
[24] Dimension 3100, Nanoscope III AFM from Veeco Instruments, Santa Barbara, CA, USA.
[25] MikroMasch, Tallinn, Estonia.
[26] D. Sarid, *Scanning Force Microscopy* (Oxford University Press, New York, 1994).
[27] M. W. Nelson, P. G. Schroeder, R. Schlaf, and B. A. Parkinson, J. Vac. Sci. Technol. B **17**, 1354 (1999).
[28] K. K. Likharev, IBM J. Res. Dev. **32**, 144 (1988).
[29] A. A. Middleton and N. S. Wingreen, Phys. Rev. Lett. **71**, 3198 (1993).
[30] J. Lambert, G. De Loubens, T. Mélin, C. Guthmann, and M. Saint-Jean, Phys. Rev. B (to be published).
[31] S. M. Sze, *Physics of Semiconductor Devices*, 2nd ed. (Wiley, New York, 1981).
[32] J. Chevrier, V. Le Thanh, R. Buys, and J. Derrien, Europhys. Lett. **8**, 737 (1991).
[33] A. Pimpinelli and J. Villain, *Physics of Crystal Growth* (Cambridge University Press, Cambridge, U.K., 1998).